Denitrification in a hypersaline lake–aquifer system (Pétrola Basin, Central Spain): The role of recent organic matter and Cretaceous organic rich sediments

J.J. Gómez-Alday [a,1], R. Carrey [b], N. Valiente [a,*], N. Otero [b], A. Soler [b], C. Ayora [c], D. Sanz [a], A. Muñoz-Martín [d], S. Castaño [a], C. Recio [e], A. Carnicero [e], A. Cortijo [a]

[a] Hydrogeology Group, Institute for Regional Development (IDR), University of Castilla–La Mancha (UCLM), Campus Universitario s/n, 02071 Albacete, Spain
[b] Grup d'Mineralogia Aplicada i Medi Ambient, Dep. Cristal·lografia, Mineralogia i Dipòsits Minerals, Facultat de Geologia, Universitat de Barcelona, C/ Martí i Franquès s/n, 08028, Barcelona, Spain
[c] Grup d'Hidrologia Subterrània (GHS), Institut de Diagnóstic Ambiental i Estudis de l'Aigua (IDAEA-CSIC), C/Jordi Girona 18, 08028 Barcelona, Spain
[d] Applied Tectonophysics Group, Departamento de Geodinámica, Universidad Complutense de Madrid, C/José Antonio Novais 2, 28040 Madrid, Spain
[e] Stable Isotope Laboratory, University of Salamanca, Plz. De los Caídos s/n, 37008 Salamanca, Spain

HIGHLIGHTS

- Denitrification comes about in a hypersaline lake–aquifer system.
- Nitrate in the basin is derived from synthetic fertilizers slightly volatilized.
- Organic carbon oxidation is likely to be the main electron donor in denitrification.
- Density driven flow transports organic carbon to deeper zones of the aquifer.

ABSTRACT

Agricultural regions in semi-arid to arid climates with associated saline wetlands are one of the most vulnerable environments to nitrate pollution. The Pétrola Basin was declared vulnerable to $NO3^{-}$ pollution by the Regional Government in 1998, and the hypersaline lake was classified as a heavily modified body of water. The study assessed groundwater $NO3^{-}$ through the use of multi-isotopic tracers ($\delta^{15}N$, $\delta^{34}S$, $\delta^{13}C$, $\delta^{18}O$) coupled to hydrochemistry in the aquifer connected to the eutrophic lake. Hydrogeologically, the basin shows two main flow components: regional groundwater flow from recharge areas (Zone 1) to the lake (Zone 2), and adensity-driven flow from surface water to the underlying aquifer (Zone 3). In Zones 1 and 2, δ15NNO3 and δ18ONO3 suggest that NO3− from slightly volatilized ammonium synthetic fertilizers is only partially denitrified. The natural attenuation of NO3− can occur by heterotrophic reactions. However, autotrophic reactions cannot be ruled out. In Zone 3, the freshwater–saltwater interface (down to 12–16 m below the ground surface) is a reactive zone for NO3− attenuation. Tritium data suggest that the absence of NO3− in the deepest zones of the aquifer under the lake can be attributed to a regional groundwater flow with long residence time. In hypersaline lakes the geometry of the density-driven flow can play an important role in the transport of chemical species that can be related to denitrification processes.

Keywords: Hypersaline lake Freshwater–saltwater interface Stable isotopes Nitrification Denitrification

1. Introduction

The European Groundwater Directive (EC, 2006) considers nitrate (NO_3^-) as one of the most significant contaminants that could prevent reaching the goals of the Water Framework Directive (EC, 2000). Exces-sive use of synthetic and/or organic fertilizers in agriculture and wastewater spill out are the principal sources of NO_3^- in the environment. High NO_3^- concentrations in groundwater are a matter of great concern due to its negative effects on health (Comly, 1945; Magee and Barnes,

1956; Fraser and Chilvers, 1981; Ward, 2005) and on the eutrophication of surface water bodies (Dassenakis et al., 1998; Mason, 2002; Kraft and Stites, 2003). The NO_3^- concentration threshold established by Directive 98/83/CE (EC, 1998) for human water supplies is 50 mg/L.

At the watershed scale, the identification of pollution sources is helpful in order to design mitigation measures. The quantification of natural NO_3^- attenuation processes provides information about the system capacity for water resource renewal. Denitrification is considered the main process that irreversibly eliminates NO_3^- from groundwater. Many studies have shown the complexity of this process in aquatic ecosystems (Piña-Ochoa and Álvarez-Cobelas, 2006). Denitrification is a redox reaction driven by specialized bacteria that utilize organic carbon disseminated in the sediment (heterotrophic denitrification) or reduced sulfur compounds (autotrophic denitrification) such as Fe^{2+} bearing minerals (i.e. Fe^{2+}-sulfides and Fe^{2+}-silicates) as electron donors for NO_3^- reduction to harmless N_2 (Korom, 1992; Appelo and Postma, 2005). Denitrification can be represented by the following chemical reactions:

$$5CH_2O + 4NO_3^- \rightarrow 2N_2 + 4HCO_3^- + CO_2 + 3H_2O \quad (1)$$

$$5FeS_2 + 14NO_3^- + 4H^+ \rightarrow 7N_2 + 10SO_4^{2-} + 5Fe^{2+} + 2H_2O. \quad (2)$$

As numerous authors have shown, the isotopic composition of dissolved NO_3^- can provide information about the source of the pollution (Böttcher et al., 1990; Vitòria et al., 2004; Widory et al., 2004; Kendall et al., 2007; Lee et al., 2008). In addition, a multi-isotopic approach coupled to hydrochemistry is a useful method for understanding denitrification reactions in aquifers and surficial water systems (Mariotti et al., 1988; Wassenaar, 1995; Aravena and Robertson, 1998; Pauwels et al., 2000; Søvik and Mørkved, 2008; Vitòria et al., 2008; among others).

Likewise, the isotopic composition of the reaction by-products (HCO_3^- and SO_4^{2-}) may be used to identify the metabolic processes involved in natural attenuation (Aravena and Robertson, 1998; Otero et al., 2009). In the case of heterotrophic denitrification, an increase in HCO_3^- concentration coupled with a decrease in $\delta^{13}C$ value and NO_3^- concentration should be expected. On the other hand, autotrophic denitrification should produce an increase in SO_4^{2-} concentration, and the $\delta^{34}S$ from dissolved sulfate should alter in tandem with the isotopic composition of SO_4^{2-} from sulfide oxidation, whereas the $\delta^{18}O_{SO_4}$ would be in equilibrium with the isotopic composition of $\delta^{18}O_{H_2O}$ according to Van Stempvoort and Krouse (1994).

Endorheic basins are closed drainage basins which permit the retention of water in lakes that has no outlet other than evaporation (Hammer, 1986). In arid and semiarid regions around the world salt lakes represent about 104,000 km^3 (0.008%) of the total volume of water in the Earth (freshwater lakes and rivers comprise about 126,000 km^3; Williams, 1996). Endorheic basins in semi-arid or arid regions are vulnerable to pollution due to their low precipitation and high evaporation rates (Lacayo, 1991; Schütt, 1998; Delle Rose et al., 2009). However, they have also shown a high potential to remove nitrogen compounds from agricultural runoff (Brinson et al., 1995). However, if the necessary conditions are met, NO_3^- can be reduced by denitrification in surface and/or groundwaters (Seitzinger et al., 2006; Schubert et al., 2006; Harrison et al., 2009; Nizzoli et al., 2010). In endorheic systems, the role of the lake in NO_3^- attenuation is linked with the interactions between high-salinity lake water and fresh groundwater. The difference in density between brine from the lake and fresh groundwater can produce a density-driven downflow towards the underlying aquifer (Zimmermann et al., 2006). The freshwater–saltwater interface has been reported to be a favorable area to reduce NO_3^- in estuarine zones (Santoro, 2010 and references therein). However, to the authors' knowledge, less attention has focused on nitrogen cycle studies in endorheic systems, especially to determine the relationship between the saline lake–groundwater interface and NO_3^- attenuation processes. The High Segura River Basin in Central Spain includes an important saline endorheic complex named the Pétrola–Corral-Rubio–La Higuera Saline Complex (about 275 km^2). A total of 19 wetlands have been identified in this saline complex (Cirujano and Montes, 1988). A representative example of such an endorheic system with a saline lake is the Pétrola Basin in the Segura River Basin (Fig. 1).

Previous laboratory work using different sediments from the basin showed the potential to promote NO_3^- attenuation at the field scale (Carrey et al., 2013, 2014). In these studies, the authors demonstrated the denitrification potential of sediments from the Utrillas Facies (a regional formation of Cretaceous age rich in organic matter and sulfides such as pyrite) and the lake bottom sediments. In this context, the aim of the present work is to explain the hydrogeologic system of the Pétrola Basin, focusing on the relationship between the saline lake and regional-scale groundwater to confirm the occurrence and magnitude of the density-driven downflow. This will be based on electrical resistivity tomography (ERT) profiles and regional hydrogeological and hydrochemical data from wells and piezometers. A second aim is to identify the source of NO_3^- in groundwater and to understand the factors controlling NO_3^- distribution in the Pétrola Basin. To do so, NO_3^- attenuation processes in the basin are studied by means of chemical and multi-isotopic techniques to confirm the role of different electron donors in the basin. The results are discussed integrating laboratory experiments (Carrey et al., 2013, 2014).

2. Material and methods

2.1. Study area

The hydrogeologic boundary of the Pétrola saline lake–aquifer system extends over 43 km^2. The climate is Mediterranean, continental, and semi-arid. Mean annual precipitation is usually below 400 mm, mainly falling during the spring and autumn. Mean temperatures range from 4.9 °C (January) to 24.2 °C (July). Farming (cultivation, raising livestock) are the main economic activities in the area. Irrigation and dry land occupy about 17 km^2, which represents 40% of the total basin surface (Database Corine Land Cover 2000). Crops are fertilized mainly using inorganic synthetic fertilizers and manure is not widely applied. The estimated nitrogen load from agricultural activities was about 10 t/km^2 $year^{-1}$ (year 2000) (ITAP, 2010). The Pétrola Basin (Fig. 1) is located in a zone vulnerable to NO_3^- pollution, where fertilizer use is restricted and under government supervision (Order 2011/7/2 CMA). Nonetheless, NO_3^- input to the lake has been quantified as reaching 3.76 t/year (Cortijo et al., 2011). Furthermore, urban wastewater, from a population of 850 inhabitants, is discharged directly into the lake untreated. These NO_3^- inputs enhance eutrophication processes and produce harmful algal blooms in Pétrola Lake.

The basin geology comprises mainly Mesozoic materials. The bottom of the sequence is formed of oolitic carbonate Jurassic rocks with porosity dominated by the fracture network. The base of the Lower Cretaceous unit corresponds to the Weald Facies and consists of argillaceous sediments overlain by sands and sandy-conglomerate sediments with intergranular porosity, which reaches the Barremian. Aptian carbonates overlie Barremian terrigenous deposits. Albian deposits (Utrillas Facies) consist of siliciclastic sands, sandy-conglomerates, and reddish to dark-gray clay to argillaceous sediments deposited over Aptian sediments. The Utrillas Facies materials comprise sandy-conglomerate sediments interstratified by gray-to-black argillaceous sediments with organic matter and sulfides contents, mainly represented by pyrite. These deposits show noticeable lateral changes in thickness throughout the Pétrola Basin (average about 7 m). Weathering processes oxidizes pyrite from the lower Cretaceous argillaceous sediments to gypsum (Gómez-Alday et al., 2004). During the late Miocene, pronounced compressional events related to the Alpine Orogeny resulted in regional uplift

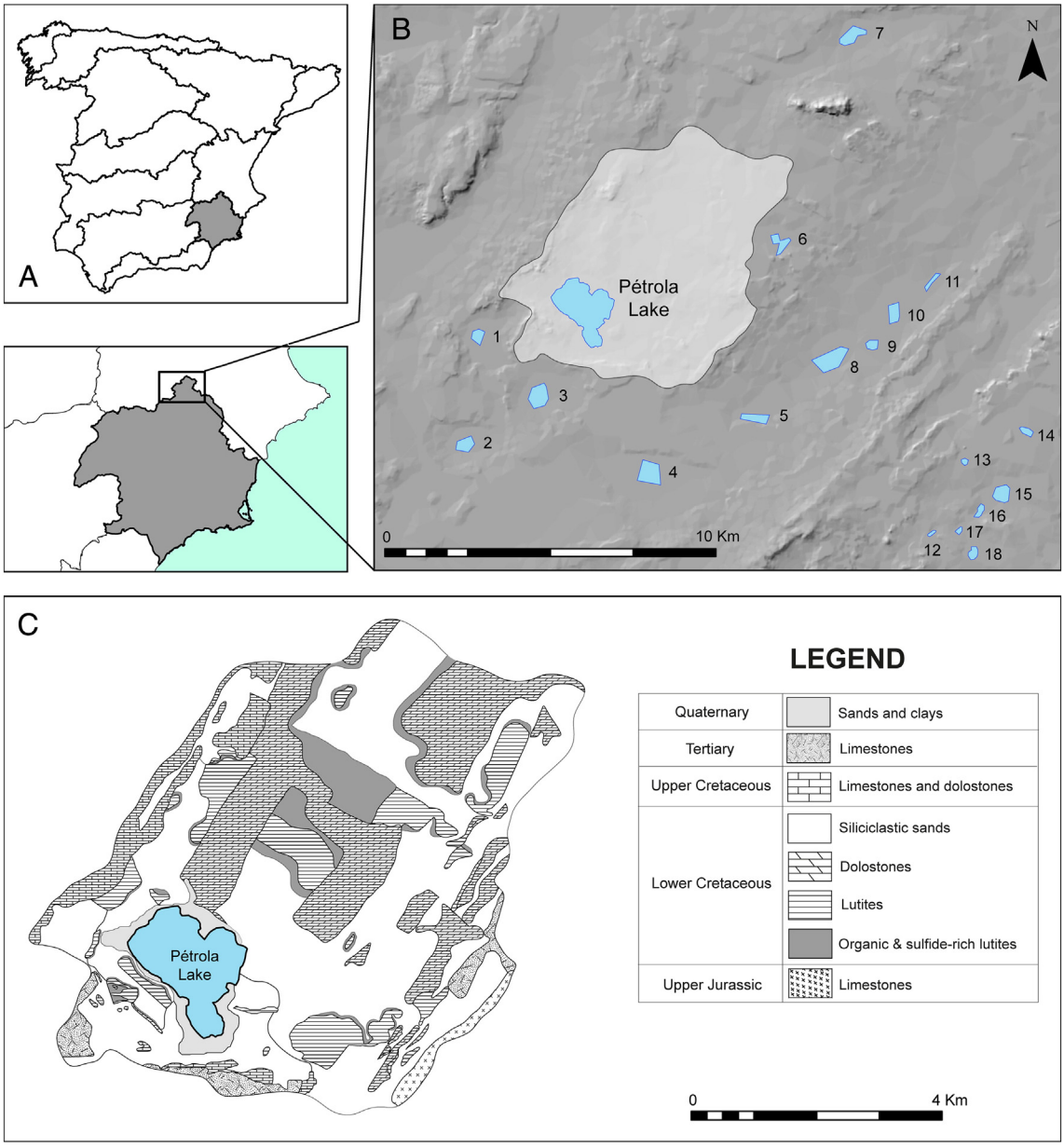

Fig. 1. A) Location of Segura River Basin. B) Pétrola–Corral-Rubio–La Higuera Saline Complex, with Pétrola Lake and other 18 wetlands: 1. Horna; 2. Casa Villora; 3. Hoya Usilla; 4. Hoya Pelada; 5. Casa Higinio; 6. El Recreo; 7. Salobrejo; 8. Hoya Grande; 9. Hoya Chica; 10. Hoya del Pozo; 11. Hoya la Huerta; 12. Hoya Elvira; 13. Mojón Blanco; 14. La Herrada; 15. El Saladar; 16. Hoya Rasa; 17. Hoya de la Yerba; 18. Atalaya de los Ojicos. C) Geological map of Pétrola Basin.

accompanied by NE–SW and NW–SE trending fractures, which produced a regional-scale horst-and-graben structure. The tectonic framework exerts important controls on the hydrogeologic system, where Pétrola Lake occupies the lower topographic position in a horst-type tectonic structure.

2.2. Field survey

A total of 154 water samples were collected from 15 control points in the Cretaceous aquifer (springs, surface water including streams and lake, and agricultural wells) between April 2008 and December 2010 (see Fig. 2). Additionally, four PVC piezometers (2623, 2624, 2625, 2626) were installed in 2008 near the lake margin in order to measure the vertical profiles of hydrogeochemical parameters at different depths in the aquifer system (Fig. 2). The piezometers were 5 cm in inner diameter, and were installed at different depths: 12.1 m (2626), 25.8 m (2624), 34.1 m (2625), and 37.9 m (2623). Screen lengths were 3 m (2623), 9 m (2624), 5 m (2625), and 4 m (2626). Screening zones were isolated by means of internal bentonite seals. A total of 27 water samples were collected from the four piezometers. In addition, 48 samples of sulfides, carbonates and gypsum from weathered pyrite from the Utrillas Facies were collected from the basin and analyzed for sulfur, oxygen, and carbon isotope composition.

Simultaneous measuring of groundwater level, temperature (T) and electrical conductivity (EC) were performed for piezometers 2624, 2625 and 2626, using ceramic CTD-Diver stand-alone sensor (piezometer 2623 was a flowing well). Data collected cover from February 2010 until November 2010, which comprises the high and the low stand state of the water level of the lake. The time intervals predetermined were 24 h. A total of 288 daily measurements were gathered.

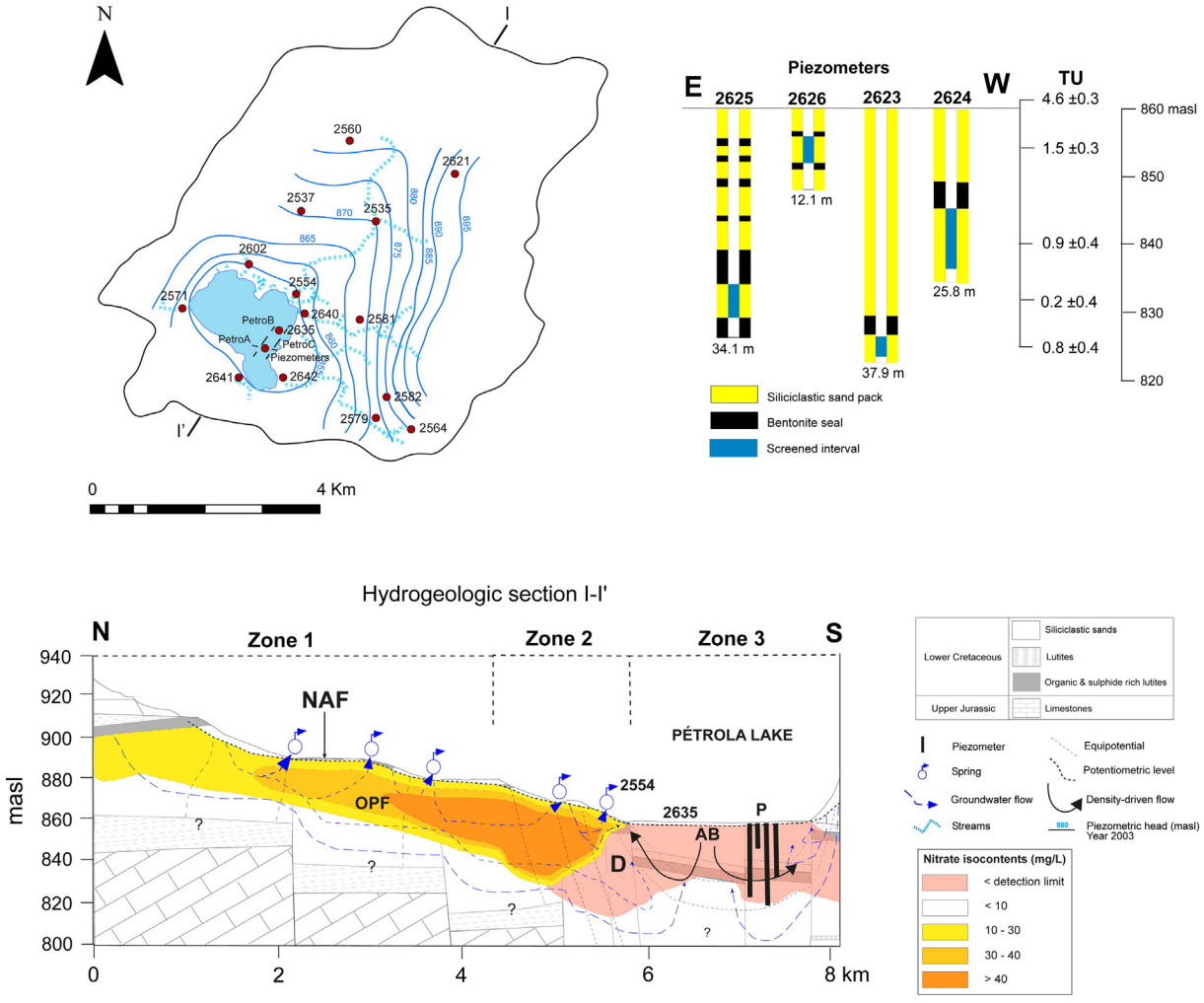

Fig. 2. Location of sample points and ERT profiles (PetroA, PetroB and PetroC) in Pétrola Basin. The simplified hydrogeological cross-section I–I′ shows the conceptual model proposed for denitrification in the hypersaline lake where organic matter can be transported by the different density-driven flow. masl: meters above sea level. NAF: nitrification of ammonium fertilizers. OPF: oxic polluted freshwaters. D: denitrification. AB: anoxic brine. P: piezometers. TU: tritium units. Contours in the contaminant plume represent estimated nitrate concentrations in groundwater.

Precipitation data for the studied period were obtained from the meteorological station AB07 (Ministry of Agriculture, Food and Environment of Spain). This station is located in Pozo Cañada, at about 16 km from Pétrola.

2.3. Chemical analyses

Groundwater T, pH, EC, redox potential (Eh), and dissolved oxygen (DO) parameters were measured in situ with portable electrodes. In the springs and streams, measurements were performed directly in the water flow, whereas in the four piezometers measurements were made using a flow-through chamber to minimize the effect of air exchange. Agricultural wells were purged prior to sampling about a minimum of three well volumes and/or until EC was stable. Water samples were stored at 4 °C in darkness prior to further analysis and following the official standard methods (APHA-AWWA-WEF, 1998). Water samples for major ions were filtered with a 0.45 μm nylon Millipore® filter. For the determination of dissolved organic carbon (DOC) samples were filtered with a 0.20 μm nylon Millipore® filter. Alkalinity titrations were carried out in the laboratory by acid–base titration. Nitrate, SO_4^{2-}, and Cl^- contents were measured by ion chromatography (DX120, Vertex). To avoid chloride interference in samples with high EC, the cadmium reduction method was employed for determining NO_3^- concentrations using a spectrophotometer (Perkin-Elmer, Lambda 650). Determination of NH_4^+ contents was carried out by distillation and volumetric methods (Koroleff method). Ca^{2+} and Mg^{2+} concentrations were measured by complexometry. The DOC concentration was determined using a Shimadzu Analyzer in the research services at the University of A Coruña.

2.4. Isotope analyses

Isotope analyses were performed following standard methodology in a subset of samples grouped according to their location and hydrogeological context. The stable isotope ratios $^{34}S/^{32}S$ and $^{18}O/^{16}O$ from dissolved SO_4^{2-} were measured on $BaSO_4$ precipitated from dissolved sulfate by the addition of 5% $BaCl_2 \cdot 2H_2O$ after acidifying the sample to pH < 2 with HCl and boiling it to prevent $BaCO_3$ precipitation, following standard methods (Dogramaci et al., 2001). The $^{34}S/^{32}S$ was also determined on Ag_2S evolved by reacting sulfides as described by Canfield et al. (1986) and Hall et al. (1988). The $\delta^{34}S$ from water samples was analyzed in a Carlo Erba Elemental Analyzer (EA) coupled in continuous flow to a Finnigan Delta C IRMS at the Centres Cientific Tècnis of

Universitat de Barcelona (CCiT-UB), whereas the $\delta^{34}S$ from gypsum and sulfide were analyzed in a SIRA-II dual inlet spectrometer at the Laboratorio de Isotopos Estables of Universidad de Salamanca (LIE-US). Gypsum and the $\delta^{18}O$ from dissolved SO_4^{2-} were analyzed in duplicate with a ThermoQuest high-temperature conversion analyzer (TC/EA) unit with a Finnigan Matt Delta C IRMS at CCiT-UB. $^{18}O/^{16}O$ ratios from H_2O were measured by the CO_2 equilibration method using a Multiflow device coupled on line to a continuous flow Isoprime Mass Spectrometer at LIE-US. $^{13}C/^{12}C$ ratios in DIC were determined on CO_2 evolved from the water by acidification with 103% H_3PO_4 employing the Multiflow device at CCiT-UB. Additionally, the HCO_3^- of a few samples was precipitated as $SrCO_3$ by the addition of 45% $SrCl_2$ to previously basified waters (to pH > 10, using NaOH). These samples were reacted with 103% H_3PO_4 in a purpose-built vacuum extraction line, and the CO_2 evolved was measured on a dual inlet SIRA-II mass spectrometer at LIE-US. The isotope composition of dissolved NO_3^- was analyzed by the bacterial denitrifier method described in Sigman et al. (2001) and Casciotti et al. (2002) at the Isotope Bioscience Laboratory (ISOFYS) of Ghent University (Belgium). Results are reported in δ values relative to international standards (Air for $\delta^{15}N$, Vienna Canyon del Diablo Triolite (VCDT) for $\delta^{34}S$, Vienna Pee Dee Belemnite (VPDB) for $\delta^{13}C$, and Vienna Standard Mean Ocean Water (VSMOW) for $\delta^{18}O$ and δD). Analytical reproducibility by repeated analysis of both international and internal reference samples of known isotopic composition was determined to be about ±1‰ for $\delta^{15}N$, ±0.2‰ for $\delta^{34}S$, ±2‰ for $\delta^{18}O$ of NO_3^-, ±0.5‰ for $\delta^{18}O$ of SO_4^{2-}, ±0.2‰ for $\delta^{13}C$, and ±0.3‰ and for $\delta^{18}O$ in water. Radioactive isotopes of H^3 (tritium) in groundwater were determined by liquid scintillation counting in ^{14}C and the Tritium Dating Service of the Autonomous University of Barcelona with an analytical reproducibility of ±0.4 TU.

2.5. Electrical resistivity tomography (ERT)

The ERT survey was carried out in 2008 when the lake was almost dry using a RESECS DMT resistivity meter equipped with 72 electrodes. The selected electrode configuration was a Wenner array because it has the highest signal-to-noise ratio and is more sensitive to vertical variations in resistivity (Loke and Dahlin, 2002). Electrode spacing was 5 m, and 23 research levels were used to reach 60 m depth in the central part of each section. Two injection cycles were applied in each measurement, taking 700 potential differences and intensity values, and calculating the root mean square error for each apparent resistivity value. Three sections, lined up on the ground surface, were measured close to the lake's eastern margin, coinciding with the industrial facilities (Fig. 2). ERT profile A (about 355 m in length) was parallel to the location of the four piezometers installed in the lake's eastern edge. ERT profiles B and C were placed perpendicular to ERT profile A, and were about 310 m and 355 m in length, respectively. As there were no noticeable differences in topography, it was not necessary to normalize profile elevations to the ground surface. Individual measurement points were revised taking into account standard deviation, RMS, and pooled standard deviation (SP). All values with a standard deviation higher than 20% were removed. Field data inversion was performed with Res2Dinv software using the same parameters in the inversion for all the profiles (deGroot-Hedlin and Constable, 1990; Loke and Barker, 1996). A least-squares inversion algorithm was chosen for inversion, and the final calculated RMS errors for the three sections were between 12% and 17%. Finally, inversion results were exported to absolute XYZ coordinates in order to compare them with hydrogeological and geochemical data.

3. Calculations

Stable isotopes are usually measured as the ratio between the less abundant isotope and the most abundant one (e.g. ^{15}N versus ^{14}N). Stable isotope ratios are reported with respect to international standards using the delta notation (Eq. (3)).

$$\delta^{15}N = \left[\left(R_{sample} - R_{std}\right)/R_{std}\right] \times 1000 \quad (3)$$

where $R = {}^{15}N/{}^{14}N$.

Throughout the nitrification processes, no isotopic fractionation occurs between the $\delta^{15}N_{NH_4}$ and $\delta^{15}N_{NO_3}$ when NH_4^+ is completely nitrified (Heaton, 1986). The $\delta^{18}O_{NO_3}$ range for nitrification was calculated using Eq. (4) (Andersson and Hooper, 1983).

$$\delta^{18}O_{NO_3} = 1/3\delta^{18}O_{O_2} + 2/3\delta^{18}O_{H_2O} \quad (4)$$

This equation can be applied when NH_4^+ is abundant and nitrification rates are high. It also assumes negligible isotopic fractionation effects during water and atmospheric O_2 ($O_{2(atm)}$) uptake (Mayer et al., 2001). It is also presumed that the $\delta^{18}O$ of O_2 used by the microorganisms is $O_{2(atm)}$. In this case, two-thirds of the oxygen atoms of NO_3^- produced are derived from water, whereas one-third is incorporated from atmospheric oxygen ($\delta^{18}O_{atm} = +23.5‰$; Dole et al., 1954).

During denitrification reactions, the isotopic composition of both ^{15}N and ^{18}O in the residual NO_3^- fraction increases as denitrification proceeds (Mariotti et al., 1981). Denitrification can be considered as a single-step Rayleigh process and isotopic fractionation (ε) can be calculated employing Eqs. (5) and (6) (Mariotti, 1986).

$$\delta^{15}N_{residual} = \delta^{15}N_{initial} + \varepsilon \ln f \quad (5)$$

$$\delta^{18}O_{residual} = \delta^{18}O_{initial} + \varepsilon \ln f \quad (6)$$

where f is the residual NO_3^- concentration divided by the initial NO_3^- level and ε is the isotopic fractionation.

4. Results

4.1. Hydrogeology

The hydrogeological system is formed by two unconnected aquifers (Gómez-Alday et al., 2004). A lower, confined aquifer, comprising highly permeable oolitic Jurassic carbonates and an upper Cretaceous aquifer composed of siliciclastic sands, conglomerates, and lutites (Utrillas Facies, Albian). According hydraulic potential differences, up to 50 m, the Jurassic aquifer is disconnected from the Cretaceous by an aquiclude formed by lutitic Weald Facies. Piezometric levels measured in the Cretaceous aquifer data points show that groundwater flow in the unconfined aquifer converges to Pétrola Lake. Near the lake, the piezometric level of the Cretaceous aquifer is close to the topographic surface and, as a consequence, several springs and streams drain the aquifer in this area. Therefore, the lake can be considered as a terminal discharge zone for overland flow as small streams form a radial pattern (Fig. 2).

The ERT survey reveals a resistivity distribution that is related to several parameters including water content, EC, mineral content, porosity, and T (Fig. 3). Therefore, the first 2 m observed in profiles correspond to the height of the dykes where the ERT survey was performed and shows unsaturated conditions. Below 2 m in depth, the system is saturated. The sedimentary sequence can be considered homogeneous in the three profiles. Changes in rock porosity can be considered negligible, although preferential flow zones have been noted in the bottom of the lake as local springs. Therefore, resistivity variations are likely related to changes in water EC. Resistivity values ranged from lower than 0.2 Ω·m at the lake surface to 20 Ω·m at depths of about 50 m below the ground surface (Fig. 3). Differences in resistivity are

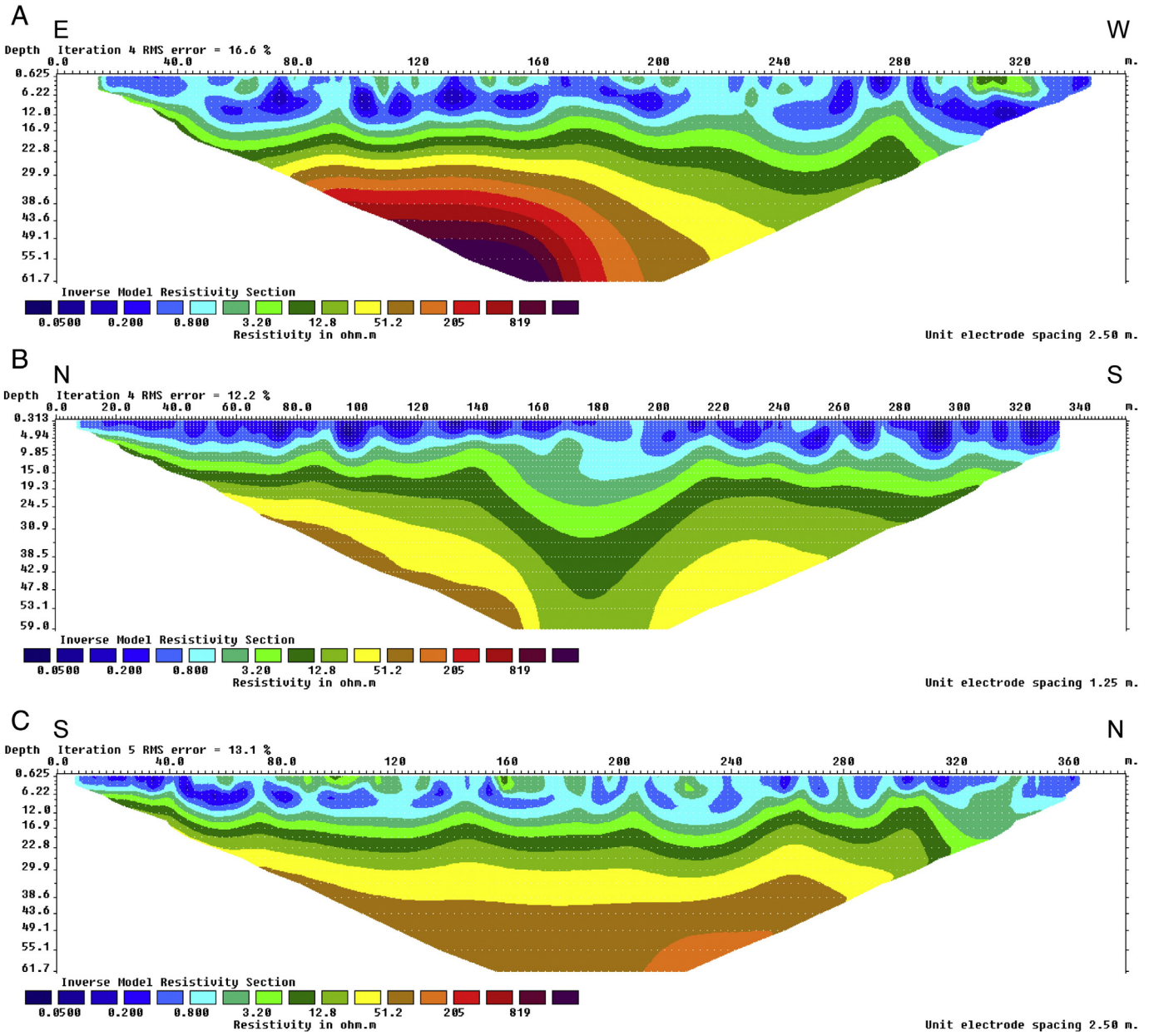

Fig. 3. Inverted resistivity sections for two-dimensional ERT profiles: A) profile PetroA; B) profile PetroB; C) profile PetroC. Data were gathered with 5 m spacing among electrodes. High resistivity (red) represents low electrical conductivity (EC), whereas low resistivity (blue) shows areas with high EC. (For interpretation of the references to color in this figure legend, the reader is referred to the web version of this article.)

explained by the fact that superficial, dense brines, are perched on less dense fresh groundwater, producing a hydrodynamically unstable situation. The resistivity gradient can be interpreted as the result of a density-driven flow caused by the instability of the saline boundary layer (Zimmermann et al., 2006). Piezometers 2626, 2625, 2624, and 2623 matches with the zone of density-driven groundwater flow, where mixing of descending surface brines and ascending regional fresh groundwater occurs.

The relationship between the aquifer and Pétrola Lake is complex. Groundwater level in 2626 piezometer shows changes mostly influenced by the water level variations of the lake, which are mainly related to local precipitation pattern (Fig. 4A). Additionally, groundwater levels in 2626 should also reflect variations in the regional groundwater flow potential, since the central part of the basin represents the base level of the aquifer. Water head in saline aquifers have to be corrected by water density (Post et al., 2007). Calculated equivalent freshwater heads showed seasonal variations for the period February 2010–November 2010 driven by changes in water density (Fig. 4C). In 2626 piezometer the lowest equivalent freshwater heads were found from February to May, where the accumulate precipitation represent a value of 186.8 mm (Fig. 4B). Then, a dramatic increase from May to September coinciding with the summer months was observed. Afterwards, equivalent freshwater heads leveled off in the maximum values. Groundwater level in 2625 piezometer largely reflects variations in the regional groundwater potential (Fig. 4A). The equivalent freshwater level reaches minimum values from June to October (Fig. 4C). The groundwater level evolution in 2624 piezometer leveled off from February to June. Then, it showed an increasing trend. The calculated equivalent freshwater level showed a declining trend from June to November. Equivalent freshwater heads suggest that the largest influence of the lake brine waters match with the lowest regional groundwater potential.

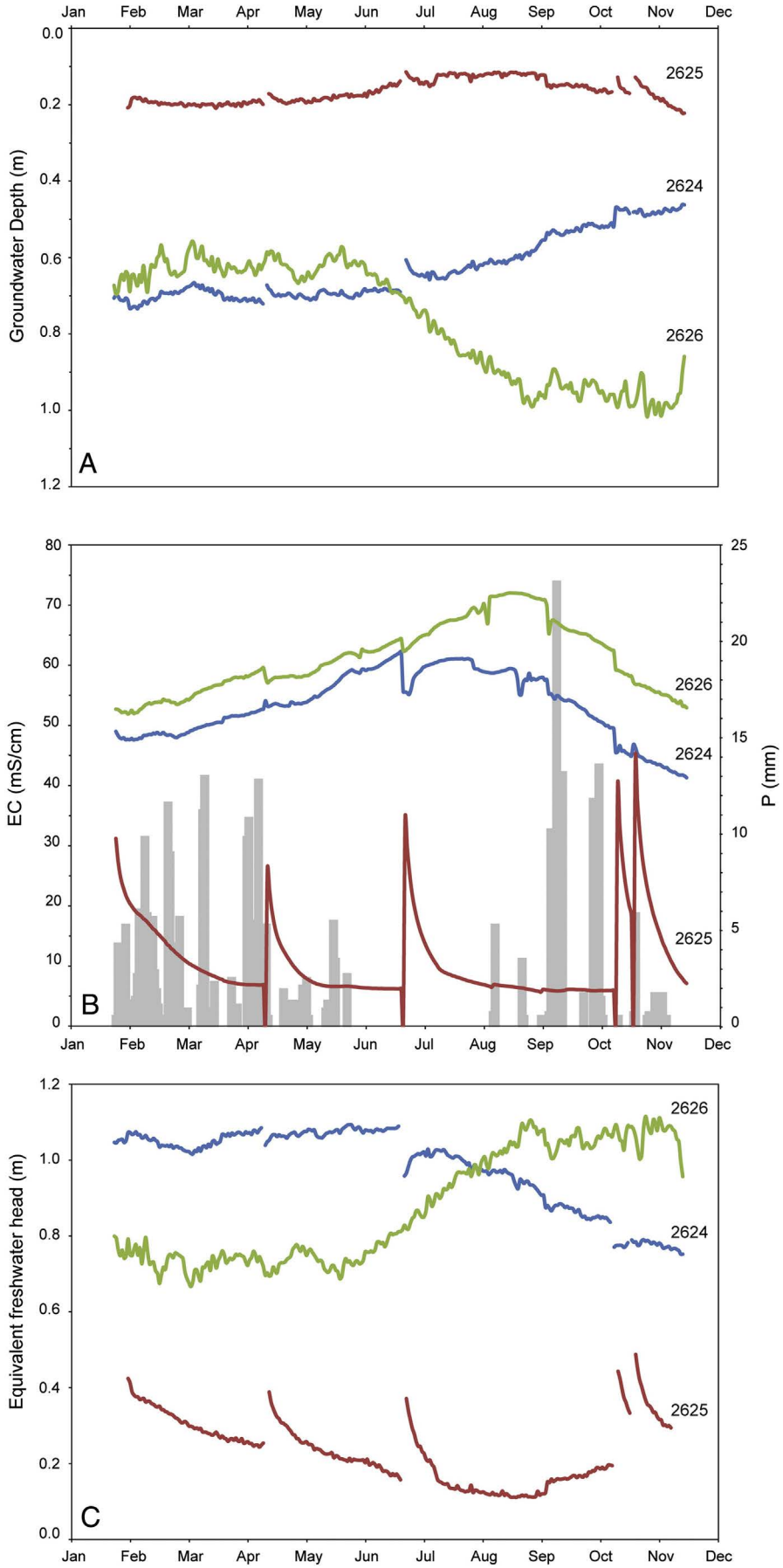

Fig. 4. Between February-2010 and November-2010, in 2624, 2625 and 2626 piezometers: A) groundwater depth; B) electrical conductivity (EC) and precipitation (P); C) equivalent freshwater head.

Table 1
Tritium activities (UT) in water samples.

Data point	Location	Sample date	UT
2564	Zone 1	30/04/2010	2.7 ± 0.4
2579	Zone 1	30/04/2010	0.7 ± 0.4
2581	Zone 1	30/04/2010	3.3 ± 0.4
2623	Zone 3	30/04/2010	0.8 ± 0.4
2624	Zone 3	30/04/2010	0.9 ± 0.4
2625	Zone 3	30/04/2010	0.2 ± 0.4
2626	Zone 3	18/06/2010	1.5 ± 0.3
2635	Zone 3	18/06/2010	4.6 ± 0.3

Tritium activities (Table 1) in water samples ranged from 0.2 ± 0.4 TU to 4.6 ± 0.3 TU (n = 8). The highest tritium activity was detected in the surface lake water (2635), reaching 4.6 ± 0.3 TU (Fig. 2). The shallowest piezometer installed at the lake's edge (2626) showed the highest tritium activity in groundwater (1.5 ± 0.3 TU). Lower tritium activities were observed in wells 2623 and 2625 (0.8 ± 0.4 TU), whereas 2625 showed 0.2 ± 0.4 TU.

The study area has been divided into three different zones (Fig. 2). Zone 1 corresponds to the recharge area of the upper aquifer in the north and east. Sample points in Zone 2 are near the lake discharge zone, following the groundwater flow direction from Zone 1. Therefore, Zones 1 and 2 are discussed together as regards the chemical and isotope evolution of groundwater in the Pétrola Basin. In contrast, Zone 3 represents the area of density-driven downflow from the lake to the underlying aquifer; the data points in this area are piezometers 2623, 2624, 2625, and 2626, and the surface water (data point 2635).

4.2. Hydrochemistry of Zones 1 and 2

The chemical analyses of water samples from Zone 1 and Zone 2 are presented in the Supplementary Information (Appendix A). The Zone 1 groundwater type varied between Mg–Ca–HCO_3 and Mg–Ca–SO_4 hydrofacies (8 control points; April 2008 to December 2010; n = 100) (Fig. 5). The pH ranged from 7.1 to 9.0, and Eh values was between +142 and +482 mV. In Zone 1, the EC ranged from 596 μS/cm to 1824 μS/cm, and the DO ranged from 0.3 mg/L to 11.0 mg/L. The NO_3^- concentration ranged from below the detection limit (<0.1 mg/L) to 149 mg/L. The NH_4^+ contents oscillated between below the detection limit (<0.1 mg/L) and 2.6 mg/L. The SO_4^{2-} concentration ranged from 39 mg/L to 804 mg/L, whereas Cl^- was between 9 mg/L and 164 mg/L. The HCO_3^- contents showed a minimum value of 83 mg/L and a maximum value of 344 mg/L. The DOC concentration ranged from 2.5 mg/L to 4.9 mg/L. Zone 2 hydrofacies were similar to those in Zone 1, ranging between Mg–Ca–SO_4–HCO_3 and Mg–Ca–SO_4 (6 control points; April 2008 to December 2010; n = 49) (Fig. 5). Water samples had higher EC values than those in Zone 1, ranging from 1504 μS/cm up to 3760 μS/cm. The DO was between 2.1 mg/L and 13.9 mg/L. Overall, the NO_3^- concentration in Zone 2 was slightly lower than in Zone 1, ranging from 5.6 mg/L to 96.0 mg/L. The NH_4^+ concentration varied from below the detection limit up to 2.1 mg/L. Sulfate ranged from 175 mg/L to 2009 mg/L, whereas Cl^- ranged from 7 mg/L up to 522 mg/L. Bicarbonate values oscillated from 119 mg/L to 572 mg/L, and DOC concentrations ranged from 3.1 mg/L to 8.5 mg/L.

Zone 2 hydrofacies were similar to those in Zone 1, ranging between Mg–Ca–SO_4–HCO_3 and Mg–Ca–SO_4 (6 control points; April 2008 to December 2010; n = 49) (Fig. 5). Water samples had higher EC values than those in Zone 1, ranging from 1504 μS/cm up to 3760 μS/cm. The DO was between 2.1 mg/L and 13.9 mg/L. Overall, the NO_3^- concentration in Zone 2 was slightly lower than in Zone 1, ranging from 5.6 mg/L to 96.0 mg/L. The NH_4^+ concentration varied from below the

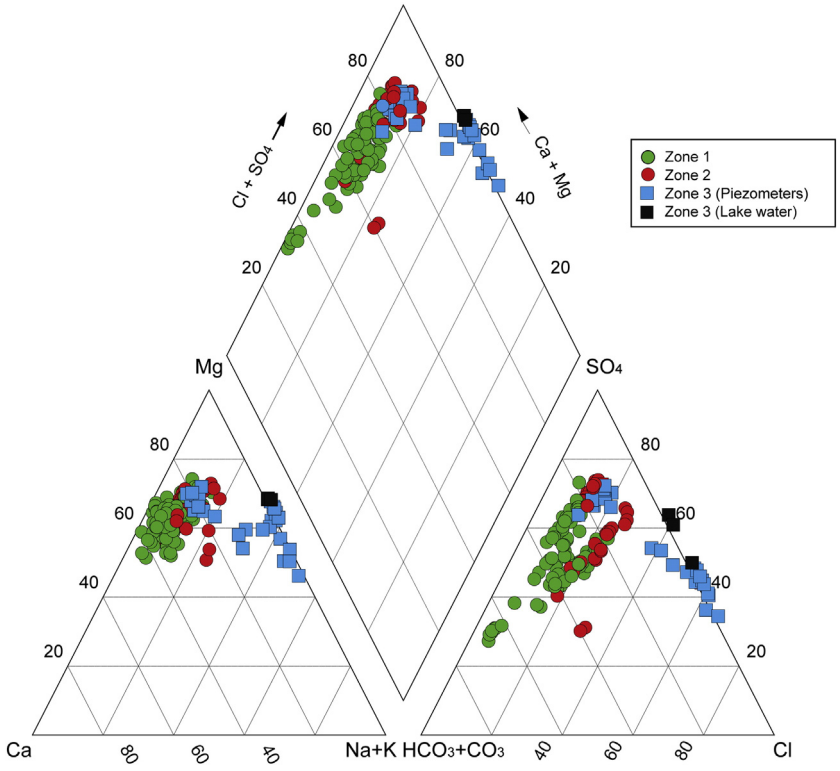

Fig. 5. Piper diagram showing the chemical composition of the surface and groundwater sample points during 2008 to 2010.

detection limit up to 2.1 mg/L. Sulfate ranged from 175 mg/L to 2009 mg/L, whereas Cl^- ranged from 7 mg/L up to 522 mg/L. Bicarbonate values oscillated from 119 mg/L to 572 mg/L, and DOC concentrations ranged from 3.1 mg/L to 8.5 mg/L.

4.3. Hydrochemistry of Zone 3

The chemical analyses of water samples from Zone 3 are presented in the Supplementary Information (Appendix A). The chemical data are displayed separately between surface water and groundwater samples from piezometers 2623, 2624, 2625 and 2626. Lake surface waters were clearly different than those in Zones 1 and 2 (Fig. 5). Hydrofacies can be classified as Mg–Na–SO_4–Cl during the study period (February 2010 to November 2010; n = 5). Lake surface waters showed a pH of 7.6 to 9.2 and an Eh of +63 mV to +292 mV. Electrical conductivity values oscillated from 59,300 μS/cm (April 2010) to 123,000 μS/cm (November 2010). Dissolved oxygen ranged from 1.1 mg/L to 5.0 mg/L. Nitrate concentration was below the detection limit (0.1 mg/L) in all the samples analyzed.

With regard to groundwater under the lake, the hydrofacies varied between Mg–Ca–SO_4–HCO_3 (2623) (comparable to Zones 1 and 2) and similar hydrofacies to the surface lake water Mg–Na–Cl–SO_4 (2626) (September 2008 to November 2010; n = 27). The pH and Eh values ranged from 6.7 to 7.6 and from −100 mV to +318 mV, respectively. EC ranged from 2540 μS/cm, in the deepest screened piezometer (2623), to 93,900 μS/cm in the shallowest one (2626). Continuous measurements of EC obtained in the piezometers between February 2010 and November 2010 showed seasonal variations in water chemistry (Fig. 4C). Electrical conductivity from 2624 and 2626 showed parallel temporal trends. The highest EC values were encountered during the summer months. Nonetheless, EC values in both piezometers were closer from February to June, with differences up to 6800 μS/cm. On the contrary, differences in EC values are more important from June to November (up to 16,900 μS/cm). In the 2625 piezometer, EC data is quite stable in time (about 6000 μS/cm). Electrical conductivity measurements suggest that the major influence of the surface water brine correspond with the lowest heads of the Cretaceous aquifer.

Dissolved O_2 ranged from 0.2 mg/L to 1.4 mg/L. NO_3^- concentrations were below the detection limit (<0.1 mg/L) in most samples except for sample point 2623, where NO_3^- showed values of up to 2.6 mg/L. Ammonium contents changed between below the detection limit (<0.1 mg/L) to 1.8 mg/L. Sulfate ranged from 510 mg/L in the deepest screened piezometer (2623) to 38,808 mg/L in the shallowest screened one (2626). Chloride concentrations varied from 82.2 mg/L (2623) to 42,012 mg/L (2626). Variations in HCO_3^- concentrations were not as noticeable: values ranged from 233 mg/L to 499 mg/L. Dissolved organic carbon contents ranged from 2.0 mg/L (2623) to 23.5 mg/L (2626).

4.4. Isotope data

The isotope analyses of water samples from Zones 1, 2 and 3 are presented in the Supplementary Information (Appendix B). These analyses were performed on a subset of samples based on NO_3^- concentrations. The $\delta^{18}O_{H_2O}$ in the water samples from Zone 1 and Zone 2 ranged from −5.4‰ to −7.6‰ (average of −6.5‰; n = 25), whereas samples from Zone 3 varied from −7.4‰ to +4.2‰ (average of −4.6‰; n = 16). The $\delta^{15}N_{NO_3}$ of the samples in Zone 1 ranged between +6.1‰ and +7.6‰ (average of +6.9‰; n = 7), and $\delta^{18}O_{NO_3}$ fluctuated between +2.1‰ and +4.7‰ (average of +3.1‰; n = 7), respectively. In Zone 2, the $\delta^{15}N_{NO_3}$ ranged from +6.6‰ to +19.9‰ (average of +12.0‰, n = 18), whereas the $\delta^{18}O_{NO_3}$ oscillated from +5.3‰ to +16.2‰ (average of +10.0‰, n = 18). The $\delta^{13}C_{DIC}$ data showed similar values in Zones 1 and 2, ranging from −5.5‰ to −1.9‰ (average of −3.2‰; n = 17). In Zone 3, the $\delta^{13}C_{DIC}$ data varied from −6.7‰ to −1.2‰ (average of −3.1‰; n = 25). The $\delta^{34}S_{SO_4}$ in the water samples from Zone 1 ranged from −17.4‰ to −12.9‰ (average of −15.0‰; n = 4), whereas $\delta^{18}O_{SO_4}$ was between +2.3‰ and +4.8‰ (average of +3.7‰; n = 4). In Zone 2, $\delta^{34}S_{SO_4}$ values ranged from −22.5‰ to −14.3‰ (average of −18.4‰; n = 6), and $\delta^{18}O_{SO_4}$ ranged between +2.9‰ and +12.3‰ (average of +7.3‰; n = 6).

Sulfide minerals (pyrite), and carbonate minerals (calcite, dolomite, and ankerite) from the basin and meteoric gypsum were also analyzed (Appendix B). The $\delta^{34}S_{gypsum}$ ranged from −30.3‰ to +3.0‰ (mean of −18.8‰; n = 15), and the $\delta^{18}O_{gypsum}$ varied from −3.2‰ to +16.4‰ (mean of 5.4‰; n = 15). The $\delta^{34}S_{sulfide}$ values from the Utrillas Facies ranged from −40.5‰ to −11.7‰ (mean of −30.4‰; n = 12). The $\delta^{13}C_{carbonate}$ analyses from the Utrillas Facies showed values ranging from −7.2‰ to +1.9‰ (mean of −1.9‰; n = 21). Ammonium concentrations ranged from 0.5 mg/L to 7.7 mg/L. Sulfate contents changed from 43,227 mg/L to 122,957 mg/L, and Cl^- varied between 21,768 mg/L and 102,814 mg/L. Bicarbonate concentrations ranged from 327 mg/L to 2135 mg/L, and DOC values varied between 140 mg/L and 646 mg/L.

5. Discussion

5.1. Nitrification and denitrification in Zone 1 and Zone 2

Since the groundwater level is usually close to the land surface, agrochemicals can rapidly reach the water table. However, NH_4^+ concentrations in Zones 1 and 2 were not significant, with a mean of 0.1 mg/L (n = 149) indicating that NH_4^+ from agricultural activities was completely nitrified to NO_3^- in the unsaturated zone. In Zone 1, higher NO_3^- values in groundwater are associated with the development of agricultural activities occurring in the basin center and southwest. There, NO_3^- concentrations increased in tandem with EC (Fig. 6). Samples in Zone 2 also showed a clear dependence of NO_3^- on EC values compared with samples from Zone 1 (Fig. 6).

More interestingly, samples from Zone 1 to Zone 2 show an increase in the isotopic composition of $\delta^{15}N_{NO_3}$ and $\delta^{18}O_{NO_3}$. Indeed, the isotopic composition of NO_3^- samples from Zone 1 showed $\delta^{15}N_{NO_3}$ and $\delta^{18}O_{NO_3}$ values falling close or inside the literature box representing NO_3^- derived from organic soil N, considering the local composition of $\delta^{18}O_{H_2O}$ (Fig. 7). Data points 2535 (average: 0.9 mg/L; n = 11), 2579 (average: 2.0 mg/L; n = 13), and 2621 (average: 1.5 mg/L; n = 9) show NO_3^- contents that could be related with organic soil N (up to 2 mg/L, Foster et al., 1982). Nonetheless, the measured NO_3^- concentration in data points 2554 and 2564 was higher than expected from an organic soil N, pointing out this origin. Nitrate from ammonium fertilizers during volatilization can reach the same $\delta^{15}N_{NO_3}$ values than organic soil N and could be the origin of nitrate in zone 1. Samples in Zone 2 have higher values of both $\delta^{15}N_{NO_3}$ and $\delta^{18}O_{NO_3}$ (>10‰) and show a positive correlation ($R^2 = 0.65$) between $\delta^{15}N_{NO_3}$ and $\delta^{18}O_{NO_3}$ (Fig. 7), indicating that denitrification processes were taking place. This observation is in agreement with observations of Carrey et al. (2013) that from laboratory experiments point out the denitrification capacity of the Utrillas sediments.

Therefore, the observed denitrification was located in the area surrounding the lake, but the attenuation was limited. In this regard, the observed denitrification at the field scale shows important spatial variability linked to variations in the amount and reactivity of labile organic matter availability, as well as a NO_3^- supply. In addition, the higher DO measured reveals the variability of the anoxic conditions in the aquifer.

5.2. Nitrate reduction in Zone 3

In continental lakes, nitrogen is one of the limiting nutrients that promote eutrophication (Vitousek et al., 1997). The important surface NO_3^- input from both farming activities and the wastewater discharged directly into the lake coupled with the increased nitrogen load from groundwater discharge have contributed to the eutrophication of the lake. In the case of Pétrola, however, NO_3^- concentrations measured in surface water are below the detection limit (<0.05 mg/L). Therefore, NO_3^- is mainly consumed in surface water by primary production, fostering seasonal algal blooms in the lake. DOC concentrations increase

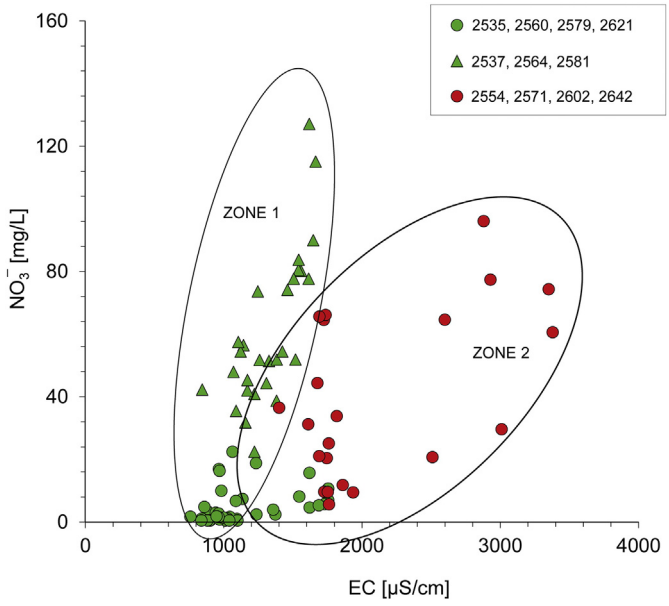

Fig. 6. Scatter plot of electrical conductivity (EC) data versus NO_3^- concentration from control points in Zone 1 and Zone 2 of the Cretaceous aquifer.

with salinity (up to 646 mg/L, October 2010), with high DOC values matching the lowest water levels in the lake (corresponding to dry periods), probably influenced by significant evaporation. This increase in organic carbon in surface lake water favors anoxic conditions (Ryther and Dunstan, 1971; Van Luijn et al., 1996). Under these circumstances, organic matter is preserved and accumulates on the lake bottom as organic-rich sediment. This significant amount of organic carbon available in surface waters can also promote NO_3^- reduction by denitrification or dissimilatory NO_3^- reduction to ammonium (DNRA) (Laverman et al., 2007). Regarding denitrification, this reaction has been observed in lakes in benthic environments or linked with lake bottom sediments (Mengis et al., 1997; Lehmann et al., 2003). In consistency with the absence of NO_3^- in the lake, the existence of the H_2S smell in the lake, and redox conditions found in the 2626 piezometer (pH ≈ 7 and Eh values up to −100 mV), suggest the presence of sulfate reducing processes, according to the redox diagram proposed by Brookins (1988). So, the NO_3^- should be reduced completely.

5.3. Quantifying denitrification

The isotopic fractionation (ε) allows quantification of NO_3^- losses due to denitrification independently of dilution and advection effects on NO_3^- concentrations. The value of ε calculated from NO_3^- isotopic composition and NO_3^- concentration can be applied to quantify the natural attenuation at the field scale (Otero et al., 2009; Torrentó et al., 2010; among others). However, using field samples, the plots of $\delta^{15}N_{NO_3}$ and $\delta^{18}O_{NO_3}$ versus $Ln[NO_3^-]$ show a poor correlation (R^2 = 0.26 and R^2 = 0.40, respectively). These poor statistical correlations can be explained due to differences in the climate conditions affecting volatilization before nitrification or mixing between different groundwater flow lines. Carrey et al. (2014) point out the denitrification capacity of organic matter-rich sediment from the bottom of Pétrola lake and determined by laboratory experiments their isotopic fractionation (ε_O = −14.5‰; ε_N = −14.7‰). These values, which not differ significantly from those obtained by Carrey et al. (2013) employing Utrillas sediments (ε_O = −11.6‰ and −15.7‰; ε_N = −12.1‰ and −13.8‰), were used to quantify the amount of NO_3^- removed by denitrification at the field scale (up to 60%). Reported average denitrification in Zone 1 reached a maximum of 10%, whereas Zone 2 showed a higher denitrification percentage, between 10% and 60% (Fig. 7). In fact, samples in Zone 2 with higher denitrification showed an average NO_3^- concentration of 44.8 mg/L, close to the human water supply threshold. For instance, sample 2602 (where the observed denitrification in 2010 was 30–40%) had a NO_3^- concentration between 46.8 mg/L and 50.4 mg/L. Even higher NO_3^- concentrations were observed at this site (96.1 mg/L in 2008 and 86.4 mg/L in 2009), illustrating that denitrification has a limited capacity to remove NO_3^-.

5.4. Identifying the electron donor for denitrification

The presence of electron donors in Zone 2 is noticeable in the organic- and sulfide-rich sediments from the Utrillas Facies (Carrey et al., 2013) and in the organic sediments of the lake bottom (Carrey et al., 2014). In the case of heterotrophic denitrification (Eq. (1)), although the distribution of HCO_3^- seems to increase as $\delta^{15}N_{NO_3}$ or $\delta^{18}O_{NO_3}$ increase, no correlation was observed between $\delta^{13}C_{DIC}$ and HCO_3^-, $\delta^{15}N_{NO_3}$, or $\delta^{18}O_{NO_3}$ because, in addition to denitrification, variations in HCO_3^- and $\delta^{13}C_{DIC}$ were also affected by carbonate dissolution and/or precipitation processes.

As concerns the oxidation of pyrite, NO_3^- attenuation by autotrophic denitrification processes could also take place (Eq. (2)). Either $O_{2(atm)}$ or water oxygen can be used during pyrite oxidation processes as electron acceptors (Taylor et al., 1984; Nordstrom and Alpers, 1999). In Zone 1, located in the north and north-east of the basin where denitrification is not observed, SO_4^{2-} concentrations show differences in spatial distribution. Most samples from the north have high SO_4^{2-} and low NO_3^- concentrations In contrast, sample points in the east (2581 and 2564) illustrate a coupled increase in NO_3^- and SO_4^{2-} concentrations. Groundwater flow through Zone 2 show a clear relationship between NO_3^- and SO_4^{2-} concentrations. The increase in SO_4^{2-} concentration can be explained by (1) pyrite oxidation in the non-saturated zone or dissolution of the meteoric gypsum formed by pyrite oxidation, and (2) pyrite oxidation during autotrophic denitrification in saturated zone.

The $\delta^{34}S_{SO_4}$ and $\delta^{18}O_{SO_4}$ isotopic composition of the dissolved SO_4^{2-} can be used to distinguish different SO_4^{2-} sources such as sulfide oxidation or evaporitic sulfate mineral dissolution (Krouse, 1980; van Stempvoort and Krouse, 1994). The Utrillas Facies is rich in reduced sulfur compounds, mainly pyrite, but in some areas secondary gypsum

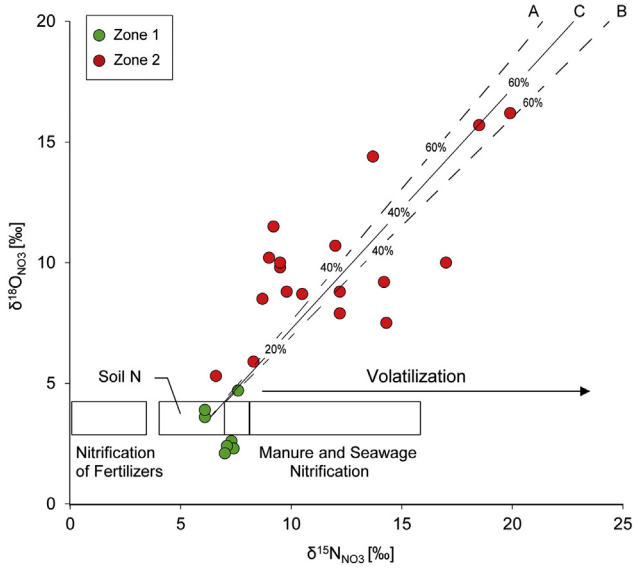

Fig. 7. $\delta^{15}N_{NO_3}$ and $\delta^{18}O_{NO_3}$ of dissolved NO_3^- in the collected samples together with the isotopic composition of the main nitrate sources: fertilizers (NO_3^- and nitrified NH_4^+ or urea), soil nitrate, and animal manure or sewage (Vitòria et al. 2004; Kendall et al., 2007; Xue et al., 2009). Dashed lines represent denitrification (%) using Utrillas sediments (A: ε_O = −12.1‰, ε_N = −11.6‰; B: ε_O = −13.8‰, ε_N = −15.7‰). Continuous line represents denitrification (%) using recent organic matter (C: ε_O = −14.5‰; ε_N = −14.7‰).

occurs from the weathering of these sulfides. The isotopic composition of disseminated sulfides in the Utrillas Facies ranges from −11.7‰ to −40.5‰. The $\delta^{34}S$ measured in gypsum located in the Utrillas Facies sediment (+3.0‰ to −30.3‰) indicates that sulfide oxidation was the main source of gypsum (Gómez-Alday et al., 2004).

Where the gypsum samples are derived from sulfide oxidation, it is impossible to determine whether the isotopic composition of dissolved sulfate originates from sulfide oxidation or from secondary gypsum dissolution, which comes also from the oxidation of pyrite, since both the $\delta^{34}S_{SO_4}$ and $\delta^{18}O_{SO_4}$ are the same values. Indeed, the groundwater samples studied have $\delta^{34}S_{SO_4}$ ranging from −12.9‰ to −22.5‰ and $\delta^{18}O_{SO_4}$ between +2.3‰ and +12.3‰, overlapping both the $\delta^{34}S$ of disseminated sulfides and the $\delta^{34}S_{SO_4}$ and $\delta^{18}O_{SO_4}$ of secondary gypsum. Even in samples affected by denitrification (2571 and 2602 from Zone 2), where sulfate could be derived from sulfide oxidation linked to denitrification, dissolved sulfate could not be isotopically distinguished from gypsum dissolution. Hence, neither chemical nor isotopic field data could completely confirm nor discard the role of sulfide in NO_3^- attenuation. Nevertheless, according to a flow-through experiment using the Utrillas Facies, where denitrification is mainly linked with organic matter, and sulfide plays a secondary role (Carrey et al., 2013).

The organic sediments from the lake bottom can also be a source of electron donors for denitrification. In the freshwater–saltwater interface, the lake brine (with no NO_3^-) mixes with fresh groundwater (contaminated by NO_3^-). Therefore, organic matter from the lake could be transported by the density-driven flow, enhancing reducing conditions and the availability of electron donors in the freshwater–saltwater interface. NO_3^- could therefore be removed in the interface. This is in agreement with the laboratory experiments performed using lake bottom sediment as an electron donor for denitrification (Carrey et al., 2014). In fact, the average NO_3^- reduction rates employing lake sediments was 1.25 mmol d^{-1} L^{-1} (maximum of 1.91 mmol d^{-1} L^{-1}) (Carrey et al., 2014), one order of magnitude higher than the NO_3^- reduction rates calculated for the organic carbon present in the Cretaceous sediments (Carrey et al., 2013).

The distribution of DOC in the piezometers shows a positive correlation with EC ($R^2 = 0.84$, Fig. 8), suggesting that labile organic matter for denitrification is available where the influence of the lake brine is more pronounced. Average DOC concentration in 2626 piezometer which was closer to lake surface waters was 20.8 mg/L. Assuming simply mixing, the participation of DOC transported by the regional groundwater flow can reach a value of 2 mg/L. The source of organic matter from the lake water would represent about 18.8 mg/L. If the distribution of DOC beyond the lake is only controlled by simply mixing processes between two ends it would result that the largest part of DOC should be linked to autochthonous (primary productivity of the lake) and allochthonous (wastewaters) sources. A minor part would be linked to autochthonous sources associated to the organic matter from Utrillas Sediments. Additionally, the high, positive, statistical relationship also suggests the secondary role of Utrillas Facies in supplying DOC to the reaction zones.

Electrical resistivity tomography profiles indicate that the freshwater–saltwater interface extends to 12–16 m below the ground surface (Fig. 3A). The conceptual model proposed, therefore, could not explain the absence of NO_3^- measured in the deepest piezometers. An alternative explanation is that the deepest piezometers are influenced by regional groundwater flow with a longer residence time and an absence of NO_3^-. Tritium in piezometer samples show no significant activity, suggesting waters infiltrating before 1950, whereas lake surface waters show higher tritium values (4.6 ± 0.3 TU), corresponding to recent recharge. Piezometer 2626 (12 m), with 1.5 ± 0.3 TU, represents a mix between surface lake water and regional groundwater, indicating the influence of the recent recharge from the lake at this depth. In the Castilla–La Mancha Region, the surface of irrigation crops began to expand in the early 1980s (Calera and Martín, 2005), so the absence of NO_3^- in the deepest part of the aquifer under the lake is related to regional groundwater flow with a longer residence time and is not linked to denitrification. Therefore, tritium data confirm that the role of DOC transported by the density-driven downflow would be restricted to the freshwater–saltwater interface in the upper part of the aquifer, in agreement with the ERT results.

According to the equivalent freshwater head values calculated in the piezometers, the observed groundwater evolution reflects temporal changes in EC related with the local climatic conditions of the area. Seasonal changes in EC would be associated to density changes in groundwater which illustrates the dynamic nature of the freshwater–saline

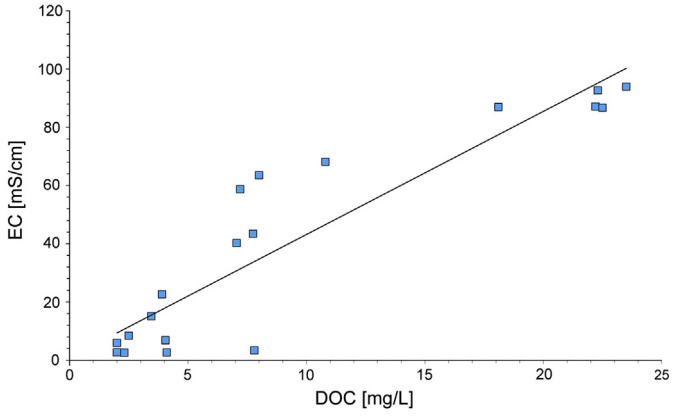

Fig. 8. Electrical conductivity (EC) values versus dissolved organic carbon (DOC) contents scatter plot ($R^2 = 0.56$) from water samples collected from piezometers in Zone 3.

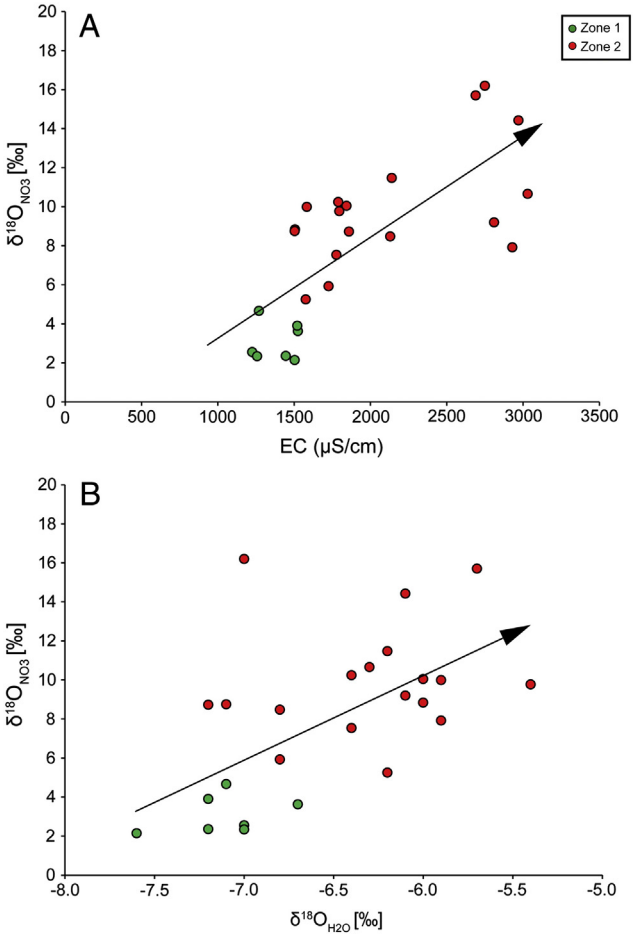

Fig. 9. A) $\delta^{18}O_{NO_3}$ against electrical conductivity (EC) values; B) $\delta^{18}O_{NO_3}$ against $\delta^{18}O_{H_2O}$ values.

water interface (Fig. 4). Denitrification in Zone 2 is also related to increasingly EC values (up to 3760 μS/cm, data point 2602) and DOC values (up to 8.5 mg/L, data point 2554). Moreover, the highest $\delta^{18}O_{H_2O}$ values tend to be located in those water points placed closer to the lake boundary. $\delta^{18}O_{NO_3}$ values increase with EC and $\delta^{18}O_{H_2O}$ (Fig. 9) which suggest that the closer distance to the lake influences the higher proportion of evaporated water and concomitantly more advanced denitrification. According to the location of data points in Zone 2, the interface can extend at distances as far as 1000 m from the lake margins. Consequently, the geometry of the freshwater–saltwater interface can play an important role in the mass transport thorough Zone 2–Zone 3.

6. Conclusions

The results obtained have important implications in understanding the role of hypersaline systems in groundwater denitrification since they can act as natural attenuation to pollution. The hydrogeologic study has shown that groundwater flow in the Pétrola Basin can be considered as the result of two main flow components: regional groundwater flow, from the perimeter area/recharge areas (Zone 1) towards the lake (Zone 2), and density-driven flow from surface water from the lake towards the underlying aquifer (Zone 3). Hydrochemical and isotope results suggest that NO_3^- reaching surface and groundwater derives from slightly volatilized ammonium synthetic fertilizers and that denitrification is taking place in the lake and the surrounding area.

Groundwater flow transporting NO_3^- intercepts two possible sources of electron donors for denitrification which can reach values of 60%: Cretaceous sediments with organic matter and sulfides, and saline waters with DOC descending from the lake. As expected from the higher reactivity of recent organic matter (Carrey et al., 2014), heterotrophic denitrification reactions were more likely to occur in zones of the saline lake–aquifer system where density-driven flow effectively transported the DOC into aquifer zones under reducing conditions. The role of DOC transported by the density-driven downflow would be restricted to the freshwater–saltwater interface in the upper part of the aquifer (down to 12–16 m below the ground surface), whereas the absence of NO_3^- in the deepest part of the aquifer is attributed to regional flow with a longer residence time. Thus, the heaviest values of $\delta^{18}O_{NO_3}$ and $\delta^{15}N_{NO_3}$ were found closer to the lake border, coinciding with higher EC and heaviest $\delta^{18}O_{H_2O}$ values suggesting that the denitrification occurs in an interface where the regional groundwater flow and the saline plume mixes. Although it cannot be completely ruled out, no evidence points to the Cretaceous sediments as a significant source of electron donors. In fact, the average NO_3^- reduction rates employing lake sediments was higher (maximum of 1.91 mmol d^{-1} L^{-1}) than those calculated for the organic carbon present in the Cretaceous sediments.

Significant spatial and temporal variability of denitrification processes within the Pétrola Basin suggests that accurate estimates of denitrification will require more extensive studies. The geometry of the density downflow can play an important role in defining the denitrification zones under the lake since it controls the distribution of reactants and products during NO_3^- reduction reactions. The 3D geometry of the mixing zone could be calculated more accurately by means of additional ETR profiles in the lake borders and the use of numerical models considering variable densities. Numerical groundwater models can be used to estimate the amount of dissolved NO_3^- which can be encountered in the zone 2 assuming not reactive processes. The results obtained could be compared with hydrochemical and isotopic data including seasonal variations.

Complete chemical and isotopic data can be found in Appendixes A and B, respectively. Supplementary data associated with this article can be found, in the online version, at http://dx.doi.org/10.1016/j.scitotenv.2014.07.129.

Acknowledgments

This work was financed by a grant (PEIC11-0135-8842) from the Castilla–La Mancha Government, the CICYT-CGL2011-29975-C04-01 and CICYT-CGL2011-29975-C04-02 projects from the Spanish Government, and the 2014 SGR 1456 project from the Catalan Government. The authors would like to thank the "Centres Científics i Tecnològics" of the "Universitat de Barcelona" and the University of Salamanca for the chemical and isotopic analyses. The authors wish to thank Christine Laurin for improving the English text and the comments from Dr. Fernando A.L. Pacheco and two anonymous reviewers for improving the manuscript.

References

Andersson KK, Hooper AB. O_2 and H_2O are each the source of one O in NO_2^- produced from NH_3 by *Nitrosomonas*: ^{15}N-NMR evidence. FEBS Lett 1983;164(no. 2):236–40.

APHA-AWWA-WEF. Standard methods for the examination of water and wastewater. Washington, DC: American Public Health Association; 1998. p. 1268.

Appelo CAJ, Postma D. Geochemistry, groundwater and pollution. CRC Press; 2005.

Aravena R, Robertson WD. Use of multiple isotope tracers to evaluate denitrification in ground water: study of nitrate from a large-flux septic system plume. Groundwater 1998;36(no. 6):975–82.

Böttcher J, Strebel O, Voerkelius S, Schmidt H-L. Using isotope fractionation of nitrate–nitrogen and nitrate–oxygen for evaluation of microbial denitrification in a sandy aquifer. J Hydrol 1990;114(no. 3):413–24.

Brinson MM, Hauer FR, Lee LC, Nutter WL, Rheinhardt RD. A guidebook for application of hydrogeomorphic assessments to riverine wetlands. DTIC document; 1995.

Brookins DG. Eh–pH diagrams for geochemistry. Springer; 1988.

Calera A, Martín F. Uso de la teledetección en el seguimiento de los cultivos de regadío. Madrid: Agua y Agronomía. Ediciones Mundi-Prensa; 2005. p. 525–81.

Canfield DE, Raiswell R, Westrich JT, Reaves CM, Berner RA. The use of chromium reduction in the analysis of reduced inorganic sulfur in sediments and shales. Chem Geol 1986;54(no. 1):149–55.

Carrey R, Otero N, Soler A, Gómez-Alday J, Ayora C. The role of Lower Cretaceous sediments in groundwater nitrate attenuation in central Spain: column experiments. Appl Geochem 2013;32:142–52.

Carrey R, Rodríguez-Escales P, Otero N, Ayora C, Soler A, Gómez-Alday J. Nitrate attenuation potential of hypersaline lake sediments in central Spain: flow-through and batch experiments. J Contam Hydrol 2014;164:323–37.

Casciotti K, Sigman D, Hastings MG, Böhlke J, Hilkert A. Measurement of the oxygen isotopic composition of nitrate in seawater and freshwater using the denitrifier method. Anal Chem 2002;74(no. 19):4905–12.

Cirujano S, Montes C. Los humedales de la provincia de Albacete, una panoramica general. Al-Basit 1988;24:77–95.

Comly HH. Cyanosis in infants caused by nitrates in well water. JAMA 1945;129(no. 2):112–6.

Cortijo A, Carrey R, Gómez-Alday J, Otero N, Soler A, Sanz D, et al. Aportes de nitrato a la laguna de Pétrola (SE, Albacete). Impacto de la agricultura y de los vertidos de aguas residuales. Congreso Ibérico sobre las aguas subterráneas (AIH-GE), Zaragoza; 2011.

Dassenakis M, Scoullos M, Foufa E, Krasakopoulou E, Pavlidou A, Kloukiniotou M. Effects of multiple source pollution on a small Mediterranean river. Appl Geochem 1998;13(no. 2):197–211.

deGroot-Hedlin C, Constable S. Occam's inversion to generate smooth, two-dimensional models from magnetotelluric data. Geophysics 1990;55(no. 12):1613–24.

Delle Rose M, Beccarisi L, Zuccarello V. Geomorphological and ecological researches inferring swamp areas inside endorheic catchment basin: the Asso graben–polje case study (south Italy). EGU General Assembly Conference Abstracts, vol. 11. ; 2009. p. 4227. [April].

Dogramaci SS, Herczeg A, Schiff S, Bone Y. Controls on δ^{34}S and δ^{18}O of dissolved sulfate in aquifers of the Murray Basin, Australia and their use as indicators of flow processes. Appl Geochem 2001;16(no. 4):475–88.

Dole M, Lane G, Rudd D, Zaukelies D. Isotopic composition of atmospheric oxygen and nitrogen. Geochim Cosmochim Acta 1954;6(no. 2):65–78.

EC. Council Directive 98/83/EC, of 3 November 1998, relative to human drinking water quality [online]. Off J Eur Communities Law 1998;330. (http://eur-lex.europa.eu/LexUriServ/LexUriServ.do?uri=OJ:L:1998:330:0032:0054:EN:PDF).

EC. Council Directive 2000/60/EC, of 23 October 2000, establishing a framework for community action in the field of water policy [online]. Off J Eur Union Law 2000;327:1–73. (http://www.boe.es/doue/2000/327/L00001-00073.pdf).

EC. Council Directive 2006/118/EC, of 12 December 2006, on the protection of groundwater against pollution and deterioration [online]. Off J Eur Union Law 2006;372:19–31. (http://www.central2013.eu/fileadmin/user_upload/Downloads/Document_Centre/OP_Resources/08_Directive_2006_118_EC.pdf).

Foster S, Cripps A, Smith-Carington A. Nitrate leaching to groundwater. Philos Trans R Soc Lond B Biol Sci 1982;296(no. 1082):477–89.

Fraser P, Chilvers C. Health aspects of nitrate in drinking water. Sci Total Environ 1981;18(no. 0):103–16.

Gómez-Alday J, Castaño S, Sanz D. Origen geológico de los contaminantes (sulfatos) presentes en las aguas subterráneas de la Laguna de Pétrola (Albacete, España). Resultados preliminares. Geogaceta 2004;35:167–70.

Hall GE, Pelchat J-C, Loop J. Separation and recovery of various sulphur species in sedimentary rocks for stable sulphur isotopic determination. Chem Geol 1988;67(no. 1):35–45.

Hammer UTSaline lake ecosystems of the world, vol. 59. Springer; 1986.

Harrison JA, Maranger RJ, Alexander RB, Giblin AE, Jacinthe P-A, Mayorga E, Seitzinger SP, Sobota DJ, Wollheim WM. The regional and global significance of nitrogen removal in lakes and reservoirs. Biogeochemistry 2009;93(no. 1–2):143–57.

Heaton T. Isotopic studies of nitrogen pollution in the hydrosphere and atmosphere: a review. Chem Geol Isot Geosci Sect 1986;59:87–102.

ITAP. Datos sobre resultados de ensayos de cultivos [online]. Instituto Técnico Agronómico y Provincial; 2010.

Kendall C, Elliott EM, Wankel SD. Tracing anthropogenic inputs of nitrogen to ecosystems. Stable Isot Ecol Environ Sci 2007;2:375–449.

Korom SF. Natural denitrification in the saturated zone: a review. Water Resour Res 1992;28(no. 6):1657–68.

Kraft GJ, Stites W. Nitrate impacts on groundwater from irrigated-vegetable systems in a humid north-central US sand plain. Agr Ecosyst Environ 2003;100(no. 1):63–74.

Krouse H. Sulphur isotopes in our environment. Handb Environmen Isot Geochem 1980;1:435–71.

Lacayo M. Physical and chemical features of Lake Xolotlán (Managua). Hydrobiol Bull 1991;25(2):111–6.

Laverman AM, Canavan RW, Slomp CP, Cappellen PV. Potential nitrate removal in a coastal freshwater sediment (Haringvliet Lake, The Netherlands) and response to salinization. Water Res 2007;41(no. 14):3061–8.

Lee K-S, Bong Y-S, Lee D, Kim Y, Kim K. Tracing the sources of nitrate in the Han River watershed in Korea, using $\delta^{15}N–NO_3^-$ and $\delta^{18}O–NO_3^-$ values. Sci Total Environ 2008;395(no. 2–3):117–24.

Lehmann MF, Reichert P, Bernasconi SM, Barbieri A, McKenzie JA. Modelling nitrogen and oxygen isotope fractionation during denitrification in a lacustrine redox-transition zone. Geochim Cosmochim Acta 2003;67(no. 14):2529–42.

Loke MH, Barker R. Rapid least-squares inversion of apparent resistivity pseudosections by a quasi-Newton method. Geophys Prospect 1996;44(no. 1):131–52.

Loke MH, Dahlin T. A comparison of the Gauss–Newton and quasi-Newton methods in resistivity imaging inversion. J Appl Geophys 2002;49(no. 3):149–62.

Magee P, Barnes J. The production of malignant primary hepatic tumours in the rat by feeding dimethylnitrosamine. Br J Cancer 1956;10(no. 1):114.

Mariotti A. Denitrification in groundwaters, principles and methods for its identification—a review. J Hydrol 1986;88(no. 1–2):1–23.

Mariotti A, Germon J, Hubert P, Kaiser P, Letolle R, Tardieux A, Tardieux P. Experimental determination of nitrogen kinetic isotope fractionation: some principles; illustration for the denitrification and nitrification processes. Plant and Soil 1981;62(no. 3):413–30.

Mariotti A, Landreau A, Simon B. ^{15}N isotope biogeochemistry and natural denitrification process in groundwater: application to the chalk aquifer of northern France. Geochim Cosmochim Acta 1988;52(no. 7):1869–78.

Mason CF. Biology of freshwater pollution. Pearson Education; 2002.

Mayer B, Bollwerk SM, Mansfeldt T, Hütter B, Veizer J. The oxygen isotope composition of nitrate generated by nitrification in acid forest floors. Geochim Cosmochim Acta 2001;65(no. 16):2743–56.

Mengis M, Gächter R, Wehrli B, Bernasconi S. Nitrogen elimination in two deep eutrophic lakes. Limnol Oceanogr 1997;42(no. 7):1530–43.

Nizzoli D, Carraro E, Nigro V, Viaroli P. Effect of organic enrichment and thermal regime on denitrification and dissimilatory nitrate reduction to ammonium (DNRA) in hypolimnetic sediments of two lowland lakes. Water Res 2010;44(no. 9):2715–24.

Nordstrom DK, Alpers C. Geochemistry of acid mine waters. Environ Geochem Miner Depos 1999;6:133–60.

Otero N, Torrentó C, Soler A, Menció A, Mas-Pla J. Monitoring groundwater nitrate attenuation in a regional system coupling hydrogeology with multi-isotopic methods: the case of Plana de Vic (Osona, Spain). Agr Ecosyst Environ 2009;133(no. 1):103–13.

Pauwels H, Foucher J-C, Kloppmann W. Denitrification and mixing in a schist aquifer: influence on water chemistry and isotopes. Chem Geol 2000;168(no. 3):307–24.

Piña-Ochoa E, Álvarez-Cobelas M. Denitrification in aquatic environments: a cross-system analysis. Biogeochemistry 2006;81(no. 1):111–30.

Post V, Kooi H, Simmons C. Using hydraulic head measurements in variable-density ground water flow analyses. Groundwater 2007;45(6):664–71.

Ryther JH, Dunstan WM. Nitrogen, phosphorus, and eutrophication in the coastal marine environment. Science 1971;171(no. 3975):1008–13.

Santoro AE. Microbial nitrogen cycling at the saltwater–freshwater interface. Hydrogeol J 2010;18(no. 1):187–202.

Schubert CJ, Durisch-Kaiser E, Wehrli B, Thamdrup B, Lam P, Kuypers MM. Anaerobic ammonium oxidation in a tropical freshwater system (Lake Tanganyika). Environ Microbiol 2006;8(no. 10):1857–63.

Schütt B. Reconstruction of Holocene paleoenvironments in the endorheic basin of Laguna de Gallocanta, Central Spain by investigation of mineralogical and geochemical characters from lacustrine sediments. J Paleolimnol 1998;20(3):217–34.

Seitzinger S, Harrison JA, Böhlke J, Bouwman A, Lowrance R, Peterson B. Denitrification across landscapes and waterscapes: a synthesis. Ecol Appl 2006;16(no. 6):2064–90.

Sigman D, Casciotti K, Andreani M, Barford C, Galanter M, Böhlke J. A bacterial method for the nitrogen isotopic analysis of nitrate in seawater and freshwater. Anal Chem 2001;73(no. 17):4145–53.

Søvik AK, Mørkved PT. Use of stable nitrogen isotope fractionation to estimate denitrification in small constructed wetlands treating agricultural runoff. Sci Total Environ 2008;392(no. 1):157–65.

Taylor BE, Wheeler MC, Nordstrom DK. Stable isotope geochemistry of acid mine drainage: experimental oxidation of pyrite. Geochim Cosmochim Acta 1984;48(no. 12):2669–78.

Torrentó C, Cama J, Urmeneta J, Otero N, Soler A. Denitrification of groundwater with pyrite and *Thiobacillus denitrificans*. Chem Geol 2010;278(no. 1):80–91.

van Luijn F, Boers P, Lijklema L. Comparison of denitrification rates in lake sediments obtained by the N_2 flux method, the ^{15}N isotope pairing technique and the mass balance approach. Water Res 1996;30(no. 4):893–900.

Van Stempvoort D, Krouse H. Controls of ^{18}O in sulfate: review of experimental data and application to specific environments. ACS Symposium Series, vol. 550. American Chemical Society; 1994. p. 446–80.

Vitòria L, Otero N, Soler A, Canals À. Fertilizer characterization: isotopic data (N, S, O, C, and Sr). Environ Sci Technol 2004;38(no. 12):3254–62.

Vitòria L, Soler A, Canals À, Otero N. Environmental isotopes (N, S, C, O, D) to determine natural attenuation processes in nitrate contaminated waters: example of Osona (NE Spain). Appl Geochem 2008;23(no. 12):3597–611.

Vitousek PM, Aber JD, Howarth RW, Likens GE, Matson PA, Schindler DW, et al. Human alteration of the global nitrogen cycle: sources and consequences. Ecol Appl 1997;7(no. 3):737–50.

Ward MH. Workgroup report: drinking-water nitrate and health—recent findings and research needs. Environ Health Perspect 2005;113(no. 11):1607–14.

Wassenaar LI. Evaluation of the origin and fate of nitrate in the Abbotsford Aquifer using the isotopes of ^{15}N and ^{18}O in NO_3^-. Appl Geochem 1995;10(no. 4):391–405.

Widory D, Kloppmann W, Chery L, Bonnin J, Rochdi H, Guinamant J-L. Nitrate in groundwater: an isotopic multi-tracer approach. J Contam Hydrol 2004;72(no. 1):165–88.

Williams WD. The largest, highest and lowest lakes of the world: saline lakes. Ver Limnol 1996;26:61–79.

Xue D, Botte J, De Baets B, Accoe F, Nestler A, Taylor P, et al. Present limitations and future prospects of stable isotope methods for nitrate source identification in surface-and groundwater. Water research 2009e;43(no. 5):1159–70.

Zimmermann S, Bauer P, Held R, Kinzelbach W, Walther JH. Salt transport on islands in the Okavango Delta: numerical investigations. Adv Water Resour 2006;29(no. 1):11–29.